International Journal of Nanomedicine

Dovepress
open access to scientific and medical research

Open Access Full Text Article

ORIGINAL RESEARCH

Magnetic Targeting of HU-MSCs in the Treatment of Glucocorticoid-Associated Osteonecrosis of the Femoral Head Through Akt/Bcl2/Bad/Caspase-3 Pathway

This article was published in the following Dove Press journal:
International Journal of Nanomedicine

International Journal of Nanomedicine downloaded from https://www.dovepress.com/
For personal use only.

Lian Duan[1]
Jianlin Zuo[2]
Fuqiang Zhang[1]
Binxi Li[3]
Zhonghang Xu[4]
Hao Zhang[3]
Bai Yang[3]
Wenzhi Song[5]
Jinlan Jiang[1]

[1]Scientific Research Center, China-Japan Union Hospital of Jilin University, Changchun, Jilin, People's Republic of China; [2]Department of Orthopaedics, China-Japan Union Hospital of Jilin University, Changchun, Jilin, People's Republic of China; [3]State Key Laboratory of Supramolecular Structure and Material, College of Chemistry, Jilin University, Changchun, Jilin, People's Republic of China; [4]Department of Gastrointestinal Colorectal and Anal Surgery, China-Japan Union Hospital, Jilin University, Changchun, Jilin, People's Republic of China; [5]Department of Stomatology, China-Japan Union Hospital of Jilin University, Changchun, Jilin, People's Republic of China

Purpose: Osteonecrosis of the femoral head (ONFH) is a chronic and irreversible disease that eventually develops into a joint collapse and results in joint dysfunction. Early intervention and treatment are essential for preserving the joints and avoiding hip replacement. In this study, a system of human umbilical mesenchymal stem cells-supermagnetic iron oxide nanoparticles (NPs) @polydopamine (SCIOPs) was constructed. The magnetic targeting system gathers in the lesion area, inhibits the apoptosis of bone cells, enhances osteogenic effect, and effectively treats ONFH under external magnetic field.

Materials and Methods: The supermagnetic iron oxide NPs @polydopamine (SPION@PDA NPs) were characterized by transmission electron microscopy and zeta potential, respectively. The effects of SPION@PDA NPs on the viability, proliferation, and differentiation of stem cells were detected by the CCK8 method, flow cytometry, and staining, respectively. The serum inflammatory indicators were detected by Luminex method. The bone mass of the femoral head was analyzed by micro computed tomography. The expression of apoptosis and osteoblast-related cytokines was detected by Western blotting. The osteogenesis of the femoral head was detected by histological and immunohistochemical sections.

Results: The SCIOPs decreased the pro-inflammatory factors, and the micro CT showed that the bone repair of the femoral head was enhanced after treatment. The hematoxylin and eosin sections also showed an increase in the osteogenesis in the femoral head. Western blotting results showed and increased expression of anti-apoptotic proteins Akt and Bcl-2, decreased expression of apoptotic proteins caspase-3 and Bad, and increased expression of osteogenic proteins Runx-2 and Osterix in the femoral head.

Conclusion: Under the effect of magnetic field and homing ability of stem cells, SCIOPs inhibited the apoptosis of osteoblasts, improved the proliferation ability of osteoblasts, and promoted bone repair in the femoral head through the Akt/Bcl-2/Bad/caspase-3 signaling pathway, thereby optimizing the tissue repair ability.

Keywords: SPION@PDA NPs, HU-MSCs, GC-ONFH, apoptosis

Correspondence: Jinlan Jiang; Wenzhi Song
China-Japan Union Hospital of Jilin University, No. 126 Xian Tai Street, Changchun, Jilin, People's Republic of China
Tel\Fax +86 431-84995432
Email jiangjinlan@jlu.edu.cn; songwz@jlu.edu.cn

Introduction

Osteonecrosis of femoral head (ONFH) occurs due to the interruption and damage of local blood supply in the femoral head, ischemia, and death of bone cells. This results in the fracture of bone trabecula and collapse of the femoral head, causing joint injury and dysfunction of hip joint activity in patients. However, the mechanism of

submit your manuscript | www.dovepress.com
DovePress
http://doi.org/10.2147/IJN.S244453

© 2020 Duan et al. This work is published and licensed by Dove Medical Press Limited. The full terms of this license are available at https://www.dovepress.com/terms.php and incorporate the Creative Commons Attribution – Non Commercial (unported, v3.0) License (http://creativecommons.org/licenses/by-nc/3.0/). By accessing the work you hereby accept the Terms. Non-commercial uses of the work are permitted without any further permission from Dove Medical Press Limited, provided the work is properly attributed. For permission for commercial use of this work, please see paragraphs 4.2 and 5 of our Terms (https://www.dovepress.com/terms.php).

glucocorticoid-associated osteonecrosis of femoral head (GC-ONFH) is yet unclear but is coupled to osteocyte death and osteogenic dysfunction. The main manifestations of the disease include osteonecrosis and cartilage collapse in the femoral head. The pathological features include apoptosis, increase in adipocytes, fat change in the bone marrow mesenchymal stem cells, decrease in osteoblast capacity, stress change in endothelial cells, and death of bone cells in the femoral head.[1] With the continuous development of medical science, glucocorticoids (GC) are widely used for the treatment of various clinical diseases. However, excessive GC is the main cause of ONFH. Some studies have shown that the incidence of GC-ONFH has been gradually increasing, and its onset age is also becoming younger.[2] Intriguingly, many diseases that use GC are not usually orthopedic but rather autoimmune, rheumatic, and rheumatoid connective tissue diseases. Notably, these diseases show a staged progression, and sustained or excessive use of GC is still needed for clinical treatment. Although total hip arthroplasty (THA) provides reliable clinical outcomes in patients with hip joint dysfunction, the limited service life and durability of the prosthesis restrict the application of the approach. Many investigators have proposed early treatment methods to preserve the joints, including the use of drugs,[3–5] cytokines and platelet-rich plasma (PRP),[6,7] and simple core depression (CD) of the femoral head with/without autologous bone marrow mesenchymal stem cell (BMSC) transplantation. Although these plans have provided some curative effect on GC-ONFH, and the effect is yet unsatisfactory.

Currently, the mechanism of GC-ONFH is found to be related to apoptosis of osteocytes and osteoblasts, which plays a crucial role in disease progression in the early stage of ONFH.[8–10] Firstly, glucocorticoids prevent bone resorption by inhibiting the recruitment of osteoclast precursors and reduce the proliferation and activity of osteoblasts, which disrupt the balance of osteoblasts and osteoclasts, leading to the degeneration of bone matrix.[11,12] Secondly, GC induces apoptosis of osteoblasts and osteocytes and prolongs the survival of osteoclasts, which in turn, reduces bone density, increases bone fragility, and causes tiny fractures, resulting in bone remodeling disorders.[11,13] The prolonged use and large doses of glucocorticoids caused apoptosis via the mitochondrial pathway,[14] which is regulated by AKT and Bcl family proteins. Akt is a potent inhibitory signal for apoptosis that is activated by several members of the Bcl-2 and caspase families. As Akt inhibits pro-apoptotic mediators such as Bad, the Bcl-2 expression is enhanced and that of caspase-3 is inhibited.[15,16] In addition, GC-ONFH was antagonized by osteogenic genes, *Runx-2* and *Osterix*, which are transforming factors in the regulation of morphological changes of preosteoblasts that develop into mature osteoblasts.[17] Reportedly, *Runx-2* and *Osterix* affect the maturation of osteoblasts and osteoclasts,[18] which is valuable in healing the ONFH by promoting osteogenesis. Several studies are currently focused on MSC therapy.[19] Because of their important contribution to bone disease, MSCs have recently been found to have the potential to promote bone healing. The source of stem cells is the BMSCs,[20] which are isolated from the bone marrow in an excruciating process, albeit with a low yield. In this study, human umbilical cord mesenchymal stem cells (HU-MSCs) were used as stem cell sources. Compared to the other stem cell types, HU-MSCs have the advantages of convenient drawing, low immunogenicity, and stable expansion.[21] HU-MSCs have been used in the treatment of diabetes, liver fibrosis, and other diseases, and caused no immune response or rejection of the host.[22] However, although MSC-mediated bone healing has shown great promise, the efficacy was not adequate as some lesions were located in difficult to access sites, such as the heart, spinal cord, and joints. Therefore, how to recruit stem cells to the injured site is the main issue that limits the application of stem cells. In order to optimize MSC delivery and retention, the magnetic targeting (MT) technique offers attractive possibilities in biomedicine. It was initially developed to optimize chemotherapeutic procedures and is based on prior magnetization of MSCs followed by in vivo targeting with the aid of magnetic fields, which would enable a larger proportion of inoculated cells to reach the site of injury.[23] Several investigators have explored the potential of SPION@PDA in improving the ability of drug-targeting tumor, enhancing the drug efficacy, and diagnosing and treating diseases.[24–26]

Therefore, HU-MSCs-loaded polydopamine-coated superparamagnetic iron oxide nanoparticles (NPs) (SPION@PDA) were designed as a treatment strategy. These NPs can be incorporated into the cells and afford a safe and reliable means of targeting. SPION has been widely used in the drug delivery system, MRI photographic developer, photothermal therapy, and magnetic targeting therapy due to its excellent properties.[27] Dopamine (DA) is a natural chemical neurotransmitter that can spontaneously form a polydopamine layer through in situ auto polymerization.[28,29] SPION@PDA has a unique shell-core structure and is the most practical choice for magnetic targeting due to several factors, such as high magnetic moment, affordability, availability, biocompatibility,

tunable cellular uptake, and low toxicity.[27] Based on these factors, the current study confirms the hypothesis from the following method, as shown in Figure 1, supermagnetic iron oxide NPs @polydopamine (SCIOPs) were recruited to magnetically-guided areas in a non-invasive and controllable manner under magnetic field targeting. Therefore, a large number of MSCs can deliver abundantly to the osteonecrosis part of the femoral head, which leads to more stem cells participating in the repair of ONFH, thereby fully utilizing the repair function of MSCs; thus, this phenomenon would provide a novel feasible strategy for preventing and repairing GC-ONFH.

Materials and Methods

Preparation and Characterization of Iron Oxide NPs

Fe_3O_4 NPs were prepared as follows: 2 mmol ferric acetylacetonate [$Fe(AcAc)_3$, 99%], 5 mmol 1.2-hexadecanedio (90%), 6 mmol oleylamine (olA, 70%), 6 mmol oleic acid (OA, 99%), and 70 mL benzyl ether (99%) were mixed and reacted by heating under the protection of N_2. After washing, 4 mL of 7 mg/mL Fe_3O_4 NPs was added to the aqueous solution of sodium dodecyl sulfate (SDS, 99%), and then heated to evaporate toluene. The modified NPs were distributed in Tris buffer (pH=8.5), and 1 mL of 6 mg/mL DA aqueous solution was added and mixed to obtain SPION@PDA.

Hemolysis Test

The blood of female Sprague–Dawley (SD) rats was collected into an anticoagulation tube, diluted into a concentration of 2% (1 mL:49 mL) fresh red blood cells: phosphate-buffered saline (PBS, Gibco, Gaithersburg, MD, USA) and used as the test object. The deionized water and PBS were used as positive and negative controls, respectively. SPION@PDA was diluted to various concentrations (12.5, 25, 50, 100 μg/mL) with PBS. The blood and SPION@PDA were mixed to 1 mL at a ratio of 1:1, incubated at 37 °C for 2 h, and centrifuged at 1000 rpm. The absorbance of the supernatant was measured at 545 nm using a microplate reader (Bio-Rad Laboratories Inc., Hercules, CA, USA). The hemolysis rate was calculated by the following detection formula: hemolysis rate = (Am-A0)

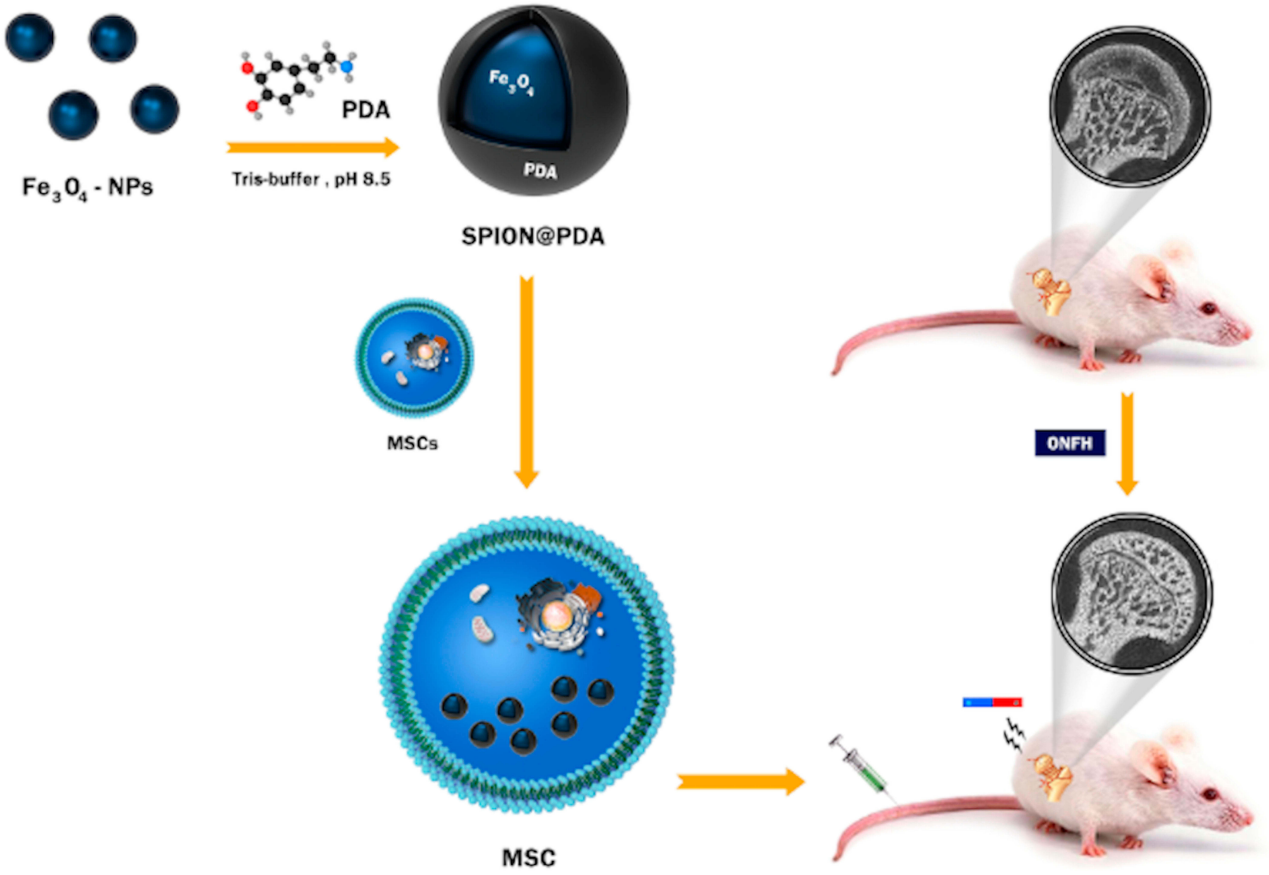

Figure 1 Research design: SPION@PDA nanoparticle preparation and internalization by MSC. GC-ONFH rats were injected MSCs through the tail vein.

/(A1-A0) × 100%. Am was the value of each detected concentration on the microplate reader. A1 was the positive control, and A0 was the negative control.

Isolation and Culture Identification of MSCs

The use of human umbilical cord in this study was approved by the Ethics Committee of China-Japan Union Hospital of Jilin University. Patients provided written informed consent. The umbilical cord was washed three times in a culture dish containing precooled 0.01 mmol/L with penicillin-streptomycin (Gibco, Gaithersburg, MD, USA) and cut into 2-cm segments. The umbilical cord was cut open to remove the artery and vein vessels, followed by obtaining Wharton's jelly and washing in PBS containing penicillin-streptomycin. Then, the cord was cut into tissue blocks of about 5 mm × 5 mm × 5 mm and inoculated at an interval of 3 mm on each piece in a 10-cm culture dish. Subsequently, 2–3 mL DMEM medium containing 20% FBS (Thermo Fisher Scientific, Waltham, MA, USA) was added, and then the tissues were cultured in 5% CO_2 at 37 °C in a humidified incubator. The medium was changed every 3 days. When the cells around the tissue block reached 70–80% confluency (16–20 days), the cells were passaged.

Intracellular NPs, Cell Viability Determination, and Proliferation Assay

Various concentrations of SPION@PDA were added to the MSCs that were cultured to a confluency of 85%. After co-incubation for 24 h, MSCs were treated according to the protocol of Prussian Blue Staining Kit (Solarbio Science and Technology, Co. Ltd, Beijing, China). Then, the MSCs were fixed 4% paraformaldehyde for 10 min, washed three times with PBS, dyed for 10 min by the staining solution, and observed under an inverted optical microscope (Olympus, Tokyo, Japan) to observe the particles entering the cells. Transmission Electron Microscope (TEM) analysis was used to observe the intracellular localization of the SPION@PDA NPs. The cells were incubated with SPION@PDA NPs (50 μg/mL) for 24 hours, and then collected and fixed in 4% glutaraldehyde for 2 hours. The ultrastructural features were observed using TEM (TEM, Jeol, Akishima Tokyo, Japan).

Cell Counting Kit 8 (CCK8, Beyotime, Shanghai, China) was used to determine the effect of SPION@PDA on the viability of HU-MSCs. Cells at a density of $1x10^4$ were inoculated into each well of 96-well plates and cultured in an incubator at 37 °C in 5% CO_2 for 24 h. Different concentrations of SPION@PDA (12.5, 25, 50, 100, 200 μg/mL) were then added. After co-incubation at 37 °C for 24 h, 10 μL CCK8 was added. The absorbance of each well was measured at 450 nm on a microplate reader (Bio-Rad Laboratories Inc.). The test was repeated four times at each concentration. For further verification, flow cytometry was performed to verify the results at the same concentration, The cells were then incubated at 4°C until flow cytometry analysis (FC500; Beckman Coulter Inc., Fullerton, CA, USA). 50 μg/mL SPION@PDA, which showed minimal toxicity, was used for the remaining tests conducted in vivo and in vitro.

Next, $5x10^3$ cells were inoculated into each well of 96-well plates. CCK8 method was used to detect the effect of 50 μg/mL SPION@PDA at different time points (24, 48, 72, and 120 h) on HU-MSCs. The absorbance of each well was measured at 450 nm on a microplate reader (Bio-Rad Laboratories Inc.). The test was repeated four times at each time point to determine the proliferative ability.

Transwell Migration Assay

Approximately, $5x10^4$ MSCs labeled with various concentrations of SPION@PDA were seeded into the upper chamber of the membrane inserts in media containing 1% FBS, which were placed into the wells of a 24-well plate (FluoroBlokTM; 8.0-μm colored PET membrane; BD Biosciences, ME, USA). The bottom chambers were filled with the growth medium containing 10% FBS. After 24 h, the upper layer of the membrane was scrapped, and the MSCs at the lower layer were fixed with 4% paraformaldehyde for 10 min, stained with hematoxylin and eosin (H&E; Sigma-Aldrich, Shanghai, China) for 10 min. The migrated cells were counted under an optical microscope (Olympus, Tokyo, Japan).

Detection of Stem Cell Characteristics

The cells ($1x10^5/cm^2$) suspensions were incubated with antibodies against CD44-phycoerythrin (PE), CD34-PE, CD105-fluorescein isothiocyanate (FITC), and CD45-FITC, respectively (all from BD Bio-Sciences, San Jose, CA, USA), in the dark for 30 min at 4 °C. The fluorescence intensity was measured using flow cytometry. To evaluate the differentiation potential, the stem cells were inoculated into 12-well plates at a density of $5×10^3/cm^2$ according to the manufacturer's protocol for the differentiation-inducing medium. Osteogenesis, adipogenesis, and chondrogenesis media (differentiation kits from Gibco, Thermo Fisher

Scientific, Waltham, MA, USA), were used to culture the cells for 21 days (osteogenesis) and 28 days (adipogenesis, chondrogenesis). The osteogenesis, adipogenesis, and chondrogenic differentiation abilities of stem cells loaded with or without SPION@PDA NPs were detected by Alizarin Red, Oil Red O, and Alcian blue staining kits, respectively (Shanghai Yuanye Bio-Technology Co., Ltd, Shanghai, China).

Labeling Procedure

Chloromethyl-benzamidodialkylcarbocyanine (CM-DiI, Life Technologies, Thermo Fisher, Carlsbad, CA, USA) was used as labeling agent. First, the cells (1×10^6 MSCs/dish) were trypsinized and distributed over 15mL tubes. 1 mg of CM-DiI was reconstituted in 1mL DMSO (Solarbio, Beijing, China) to make a stock solution. The CM-DiI stock solution (100μL) was added in 1 mL of PBS and immediately combined with the cell suspension. We used incubation times of 2 min for label.The cells were then incubated for another 30 min on ice. After incubation, the reaction was stopped by adding 5 mL of PBS, and the cells were washed and centrifuged, the cells are stored in a low temperature and dark environment until injected into the animal.

Animals and Experimental Groups

The animals were treated according to the ethical guidelines of Jilin University after obtaining approval from the Animal Welfare and Research Ethics Committee of Jilin University (experiment no. 201802060). All animal experiments were conducted in specific pathogen-free conditions (SPF) of the animal laboratory. In this study, 60 female 8-week-old SD rats weighing 220–250 g were used and randomly divided into 5 groups, with 12 rats in each group: (1) blank control group (n=12): the rats were treated with normal saline; (2) GC control group (n=12): 2 days after intravenous injection of 10 μg/kg/d lipopolysaccharide (LPS, Sigma-Aldrich, Shanghai, China), the rats were injected with 20 mg/kg/d methylprednisolone (MPS, Pfizer Manufacturing NV, Belgium) in the muscle over the femoral head for 3 days; (3) treatment group: after the model was established by LPS and MPS, the rats were divided into the following groups: (3.1) HU-MSCs treatment group (n=12); (3.2) SCIOPs treatment group (n=12); (3.3) SCIOPs under magnetic field treatment group (n=12). Each group was further divided into 3 subgroups: short-term subgroups (1 month, n=4/group), medium-term subgroup (2 months, n=4/group), and long-term subgroup (3 months, n=4/group).

One month after the models were established, rats in the 3.1 HU-MSCs group were intravenously injected with 1×10^6 MSCs/250 g (dissolved in 1 mL of normal saline), rats in the 3.2 SCIOPs group were intravenously injected with 1×10^6 MSCs/250 g (dissolved in 1 mL normal saline, SPION@PDA concentration was 50 μg/mL), and rats in the 3.3 SCIOPs under magnetic field group were intravenously injected with 1×10^6 MSC/250 g (dissolved in 1 mL normal saline, SPION@PDA concentration was 50 μg/mL). A permanent neodymium-iron-boron (NdFeB) magnet cylinder with a diameter of 20 mm (Yutong Instrument Equipment Co., Shanghai, China) was used in this study. The magnet was fixed above the femoral head of SD rats for 12 h and then removed. None of the animals died before the test, and no antibiotics were administered.

Micro CT Analysis

After euthanasia, the femoral head was dissected, the soft tissue was carefully removed, placed in 4% paraformaldehyde overnight, and scanned by Micro CT (Bruker, Skycan1172, Kontich, Belgium) at a resolution of 9 μm. The whole femoral head of each rat was scanned to evaluate the changes in the bone morphology. 3D Creator software (Volume Graphics GmbH, Heidelberg, Germany) was used to reconstruct the images. The region of interest (ROI) for analysis and comparison of parameters of the trabecula was then determined. The parameters of bone trabecula included bone mineral density (BMD), bone volume (BV), bone volume/total volume (BV/TV), bone surface/total volume (BS/TV), trabecular separation/spacing (Tb. Sp), trabecular thickness (Tb. Th), and trabecular number (Tb. N). The relative amount of bone trabeculae in the femoral head was determined.

Luminex Analysis

The rats were euthanized at different time points after 1-month interval post-treatment. The serum of SD rats was collected, and the production of specific cytokines in the serum was evaluated according to the instructions of the RnD Kit (R&D Systems Inc., Austin, Texas, USA).

Western Blot and q-PCR

The bone tissues were finely ground with liquid nitrogen. The proteins were extracted RIPA lysis buffer containing 10% PMSF and quantified using BCA Kit (Beyotime, Shanghai, China). AN equivalent of protein (80μg) was separated by 10% sodium dodecyl sulphate-polyacrylamide gel electrophoresis

(SDS-PAGE) and transferred to nitrocellulose blotting membrane (GE, Healthcare, Germany). The membrane was blocked with 5% skimmed milk powder in TBST (10 mM Tris-HCl, pH7.5, 150 mM NaCl, 0.1% Tween-20), probed with primary antibodies at 4 °C overnight, and incubated with the secondary goat anti-rabbit antibody (Li-Cor Biosciences, Lincoln, NE, USA) at room temperature for 30 min. The primary antibodies used against p-Akt (ab131443), Akt (ab38513), Bcl-2 (ab196495), Bad (ab90435), caspase-3 (ab13847), Runx-2 (ab23981), Osterix (ab209484) were purchased from Abcam (Abcam, Cambridge, UK). The immunoreactive images were acquired using the Odyssey Infrared Imaging System (LI-COR Bioscience, Lincoln, NE, USA).

TRIzol reagent (Takara Bio Inc, Kusatsu, Japan) was used to lyse the cells or tissues to obtain total RNA. The cDNA was synthesized by reverse transcription kit (TaKaRa Bio Inc., Shiga Prefecture, Japan) according to the manufacturer's instructions. SYBR (Roche, IN, USA) was used for real-time polymerase chain reaction (RT-PCR), and the relative quantification of mRNA transcripts of *Bcl-2, Bad, caspase-3, Runx-2*, and *Osterix* was determined. The β-actin gene was used as housekeeping gene. The primer sequences used for the above genes are listed in Table 1. The amplification of these genes in a 20-μL reaction was carried out using the following thermal cycle parameters: 95 °C for 10 min, 95 °C for 5 s, and 60 °C for 30 s, for a total of 40 cycles, and then at 75 °C for 30 s. The relative expression of the target genes was calculated by $2^{-\Delta\Delta Ct}$.

Table 1 Primer sequences and product sizes

Symbol	Primer Sequence	Product Size (b p)
Osterix	F-TGCAAGGCTTGATGAAGAA	160
	R-GACAGAACATAGGACAGATGA	
Runx2	F-TTGCGTGGTCAGCATGATTCG	164
	R-CTCTGGCTCGATTTCGCTTG	
Bcl2	F-CTGAAGAATGGGACAGGCATTG	176
	R-CATCACTCGTTGCATCGACC	
Bad	F-GTCAGGAAGCAGAATGGAT	156
	R-AGCACAGAGACAGTGATATG	
Caspase-3	F-AACAGGAGGAGAACCCAT	144
	R -CACCCTAACACCAGCATC	
β-actin	F-TCATGTTGGAGCCTTGGTTCTC	176
	R-CCTTGCCGGTTCTTGAGGTA	

Tissue Section Staining

The femoral head was fixed in 4% paraformaldehyde and decalcified with 10% EDTA solution for 21 days, followed by embedding in paraffin, slicing into 5-μm sections, dewaxing in xylene, rehydrating through a graded series of ethanol, and rinsing in distilled water. HE and immunohistochemical staining was performed for histological observation. Briefly, the sections were treated with 3% hydrogen peroxide in PBS for 10 min at room temperature to block the endogenous peroxidase activity. The CM-Dil Images of sections were observed using a fluorescence microscope (Olympus Corporation, Tokyo, Japan). For immunofluorescence double staining, the sections were incubated for 60 min with the appropriate antibodies. The secondary antibody goat anti-rabbit fluorescein-conjugated antibody was applied for 1 h at room temperature. All images were obtained using a fluorescence microscope (Olympus Corporation, Tokyo, Japan).

Statistical Analysis

All the experiments were repeated three times. The data were presented as means± standard deviation (SD). ANOVA was used to compare the mean values among multiple groups. An Independent sample *t*-test was used to compare the mean values between two groups. Fisher's exact test was used to compare the prevalence of disease between two groups. The statistical analyses were performed using SPSS 20.0 (IBM Co., Armonk, NY, USA). $P<0.05$ was considered statistically significant.

Results and Discussion

Characterization of SPION@PDA NPs

The poly-dopamine (PDA)-coated superparamagnetic SPION NPs were prepared by the above-described synthesis method.[23,25] The structural morphology of the synthesized NPs was initially characterized using transmission electron microscopy (TEM), as shown in Figure 2A. The average particle size of SPION was about 45–50nm, the average particle size of PDA-coated SPION was about 55–60 nm (Figure 2B), indicating that PDA was evenly coated on the surface of SPION. TEM showed that SPION@PDA NPs appeared as spherical-like particles. As shown in Figure 2C, the particle size distribution of Dynamic Light Scattering (DLS) was 146±2.3 nm,

indicating that the synthesized NPs have good homogeneity and could be attracted to the control area under the guidance of an external magnetic field (Figure 2D). To investigate the stability of the particles, the zeta potential of SPION and SPION@PDA was estimated, and the average values changed from −6.68±0.29 mV to −43.67±0.61 mV, indicating that SPION had high stability after PDA coating, and thus, it exists stably in vivo (Figure 2E). DA is a natural neurotransmitter, and in-situ auto-polymerization of PDA coating showed adequate biocompatibility,[29,30] which improved the safety of SPION NPs in biological applications. It is reported that the DA could be polymerized by oxygen in air under base environment. The DA can form thin and surface-adherent polydopamine (PDA) films onto the surface of a wide range of inorganic and organic materials via a so-called self-polymerization process.[30] In addition, the UV spectra of the synthesized and the original particles also differed significantly (Figure 2F). Collectively, the successfully synthesized SPION@PDA and PDA were selected in this study to form homogeneous shell-core nanocomposites with superparamagnetic materials, in order to improve the biocompatibility and stability of SPION.

Hemolysis, Toxicity, and Proliferation

In vitro hemolysis test is considered as a reliable and effective method to prove the blood compatibility of nanomaterials (Figure 3A). In this study, 2% fresh blood of rats was used for the test. The results revealed no hemolysis under different concentrations, and the calculated hemolysis rates were 0.012% (PBS), 0.94% (12.5μg/mL), 2.4% (25μg/mL), 4.08% (50μg/mL), and 4.82% (100μg/mL), respectively, which did not exceed the acceptable hemolysis threshold of 5% (Figure 3B). Therefore, it could be deduced that the SPION@PDA showed no hemolysis in vitro but showed hemocompatibility.

In addition, CCK8 assay was used to detect the effect of SPION@PDA at different concentrations on the activity of MSCs. SPION@PDA was co-incubated with MSCs for 24 h and detected. The findings of the viability experiments showed no significant change when compared to the blank control group if the concentration of SPION@PDA was <50 μg/mL (Figure 4A). This phenomenon indicated that the vitality of MSCs was unaffected. To further verify the effect of different concentrations of SPION@PDA on the activity of MSCs, flow cytometry was performed. Figure 4B shows

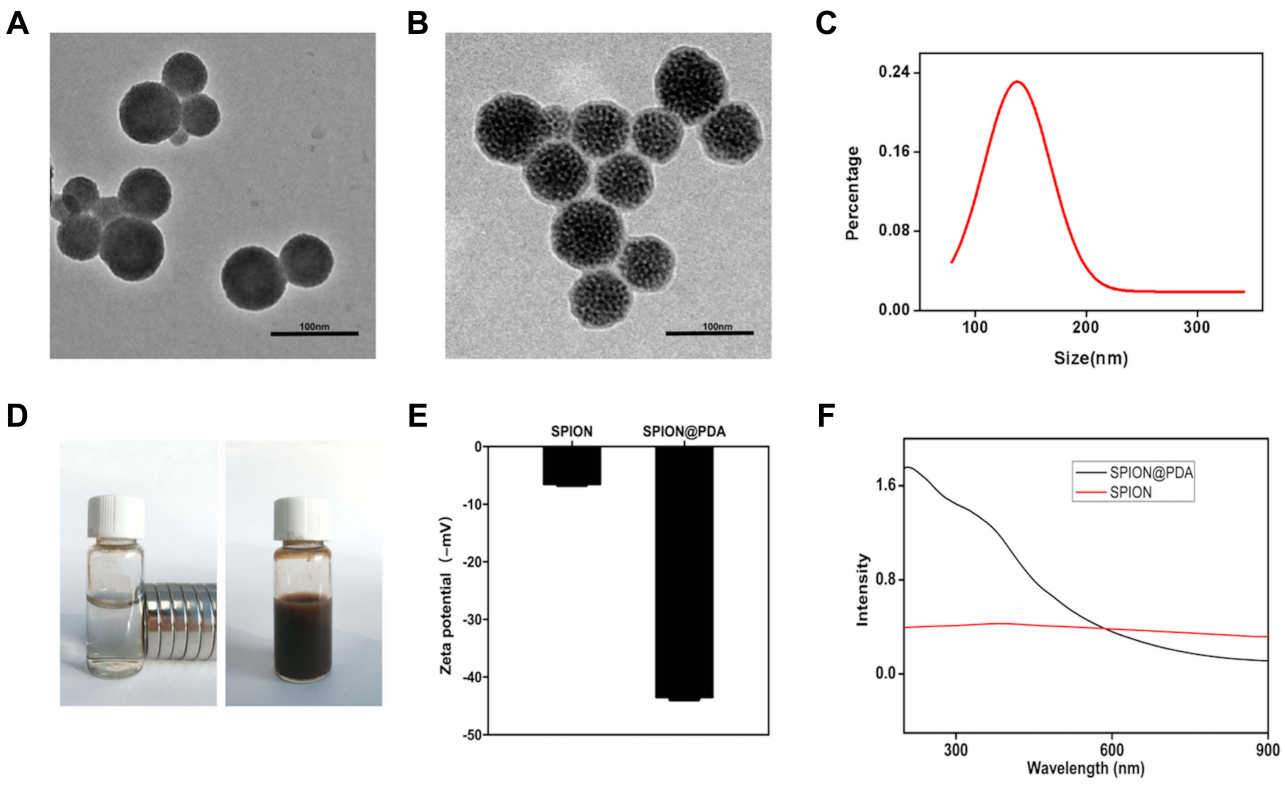

Figure 2 Characterization of SPION and SPION@PDA. (**A**) TEM image of SPION. Scale bars = 100nm. (**B**) TEM image of SPION@PDA. Scale bars = 100nm. (**C**) DLS size distribution of SPION@PDA. (**D**) SPION@PDA with or without magnetic field. (**E**) Zeta potential of SPION and SPION@PDA. (**F**) UV-vis absorption spectrum of SPION@PDA.

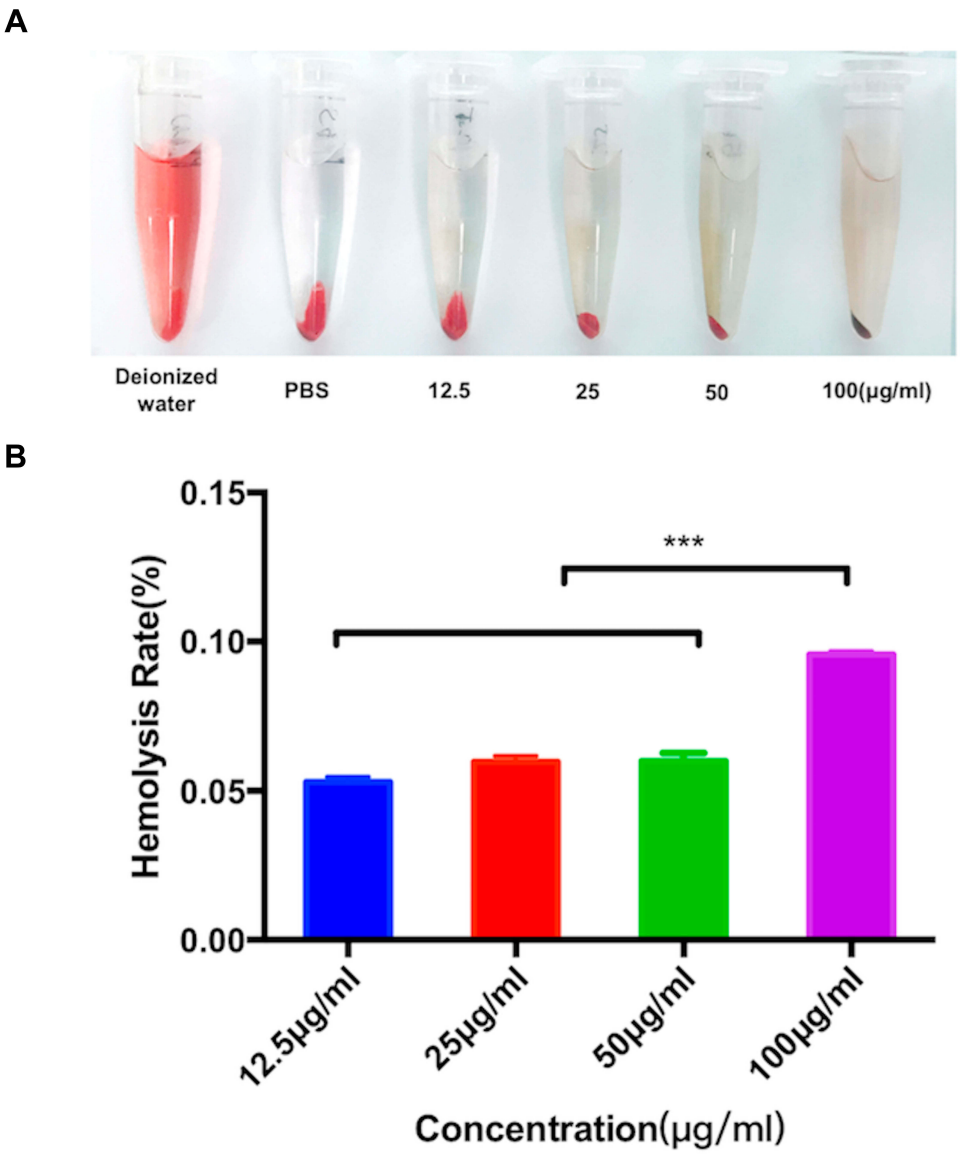

Figure 3 Evaluation of the hemolysis effect by different concentrations of the SPION@PDA NPs. (**A**) The supernatant obtained after incubating the SPION@PDA NPs in diluted fresh red blood cells. (**B**) Hemolysis rate due to different concentrations of SPION@PDA NPs, Bar represents the SD, ***$P < 0.001$.

that the concentration of 50 μg/mL did not cause apoptosis of MSCs. In summary, SPION@PDA at 50 μg/mL could be used for MSCs in subsequent experiments both in vitro and in vivo. CCK8 method was used for evaluating the 120-h proliferation test, and the results showed that the proliferation rate of SCIOPs was similar to that of the blank control group without any statistical difference (Figure 4C). The labeling efficiency and cellular uptake were analyzed by Prussian blue staining. No morphological differences were found between the labeled and unlabeled cells (Figure 4D). The labeled cells displayed the typical blue color, whereas the unlabeled cells did not exhibit the blue staining. Surface modification is an important factor that not only determines the biocompatibility of magnetic materials, but also plays a very important role in cell absorption, As shown in Figure 4E, TEM visualization was used to explore the ultrastructural features and cellular uptake of SPION@PDA. These results indicated that SPION@PDA had low cytotoxicity and good biocompatibility, and hence, was considered suitable for cell therapy.

To investigate the in vitro effect of the SPION@PDA on MSC migration, we used the transwell system and cultured MSCs with various concentrations of SPION@PDA for 24 h. The number of migrated SPION@PDA-labeled MSCs was

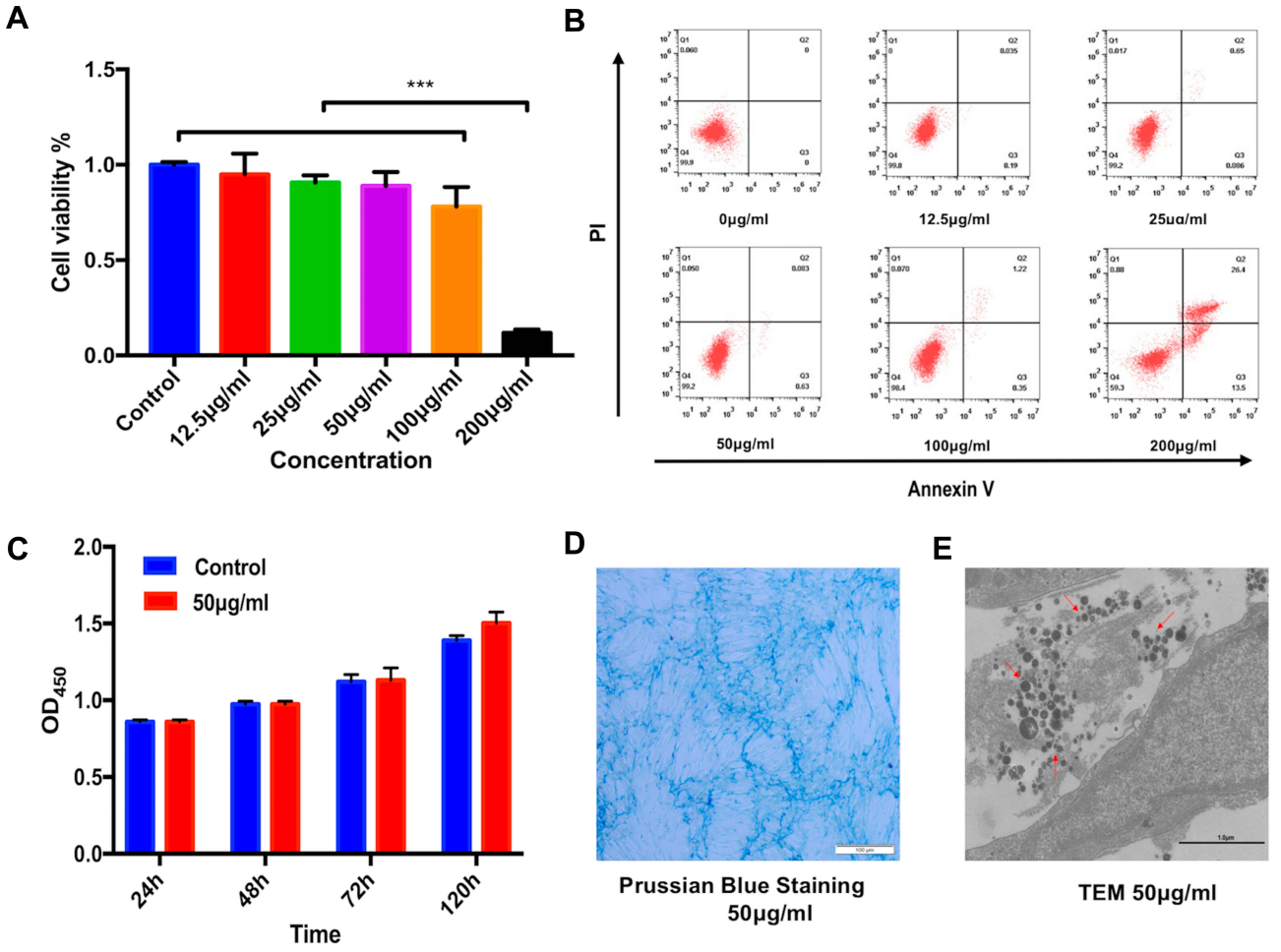

Figure 4 Viability, proliferation, and intercellular potential of the SPION@PDA-labeled MSCs. (**A**) Quantification of cell viability at varying concentrations (0, 12.5, 25, 50, 100, and 200 μg/mL) of NPs using the CCK8 assay. Bar represents the SD, ***$P < 0.001$. (**B**) Effects of SPION@PDA NPs on cell apoptosis detected by flow cytometry. (**C**) Proliferation of the MSCs labeled with SPION@PDA at 50 μg/mL for 24, 48, 72, and 120 h by CCK8 assay. (**D**) Photomicrographs showing the morphology of the MSCs labeled with the NPs at concentrations of 50 μg/mL. Scale bars = 100 μm. (**E**) TEM images at the subcellular level of SPION@PDA labeled MSCs showing some internalized NPs localized within the cytoplasm. Scale bars = 1 μm.

significantly higher than that of the control MSCs (Fig S1), thereby indicating that SPION@PDA enhances the migration of the MSCs in vitro.

Detection of Differentiation and Surface Markers of Stem Cells

To determine the osteogenesis, adipogenesis, and chondrogenesis in particles loaded with MSCs, the MSCs were used as blank control and co-cultured with SPION@PDA in osteogenesis and adipogenesis medium, respectively. Alizarin red staining, Oil Red O staining, and Alcian blue staining did not reveal any differences in osteogenesis and adipogenesis of MSCs co-cultured with SPION@PDA as compared to the control group. The osteogenic alkaline phosphatase (ALP) staining area represented the degree of osteogenesis, and no difference was detected in the size and area between the two groups. Also, no difference was detected in the number and size of the intracellular lipid droplets in Oil Red O-positive cells, indicating that the osteogenesis, adipogenesis, and chondrogenesis potential of the stem cells was unaffected (Figure 5A). To further identify the effect of SPION@PDA on the characteristics of stem cells, the typical markers on the surface of stem cells were analyzed by flow cytometry, including the typical MSC markers that are expressed in most of the MSCs CD44 (100%), CD105 (99.9%), and low expressed hematopoiesis markers CD34 (0.5%) and CD45 (0.9%) (Figure 5B). The results showed that the expression of characteristic surface markers did not alter with the application of SPION@PDA. In summary, SPION@PDA did not exert any effect on the characteristics of MSCs, and the stem cells still demonstrated the characteristics and the ability of homing to the lesion site and repairing the tissues in vivo.

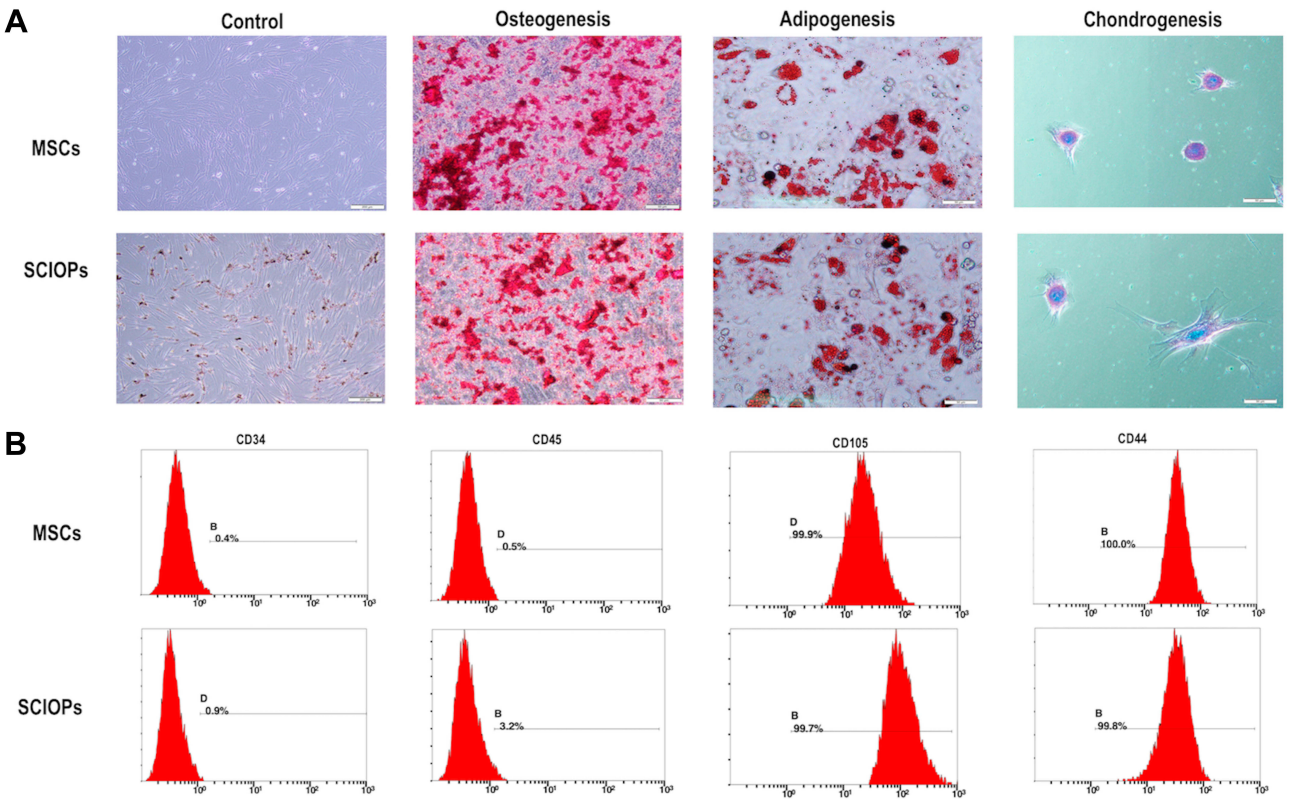

Figure 5 MSCs labeled with 50 μg/mL NPs for 24 h. (**A**) Differentiation of SPION@PDA cultured in specific differentiation media, MSCs differentiated into osteoblasts, adipocytes, and chondrocytes. (**B**) Flow cytometry analysis of SPION@PDA showed that negative for CD45 and CD34 strongly expressed typical surface antigens, such as CD44 and CD105.

Therefore, it is possible to construct the magnetic targeting system for in vivo application.

If magnetic targeting is consider to be used in the clinic, it must be shown that it is achievable with human cells, that these cells retain their regenerative properties and that an increased therapeutic effect is seen above nontargeted therapies. SPION-labeled MSC may provide some answers to these safety and available questions.

Quantitative Indicators of Femoral Head by Micro CT

For studying the effect of SCIOPs under the magnetic field on GC-ONFH, ONFH rat models were established by intravenous injection of LPS and intramuscular injection of MPS, followed by intravenous administration of HU-MSCs, SCIOPs, and SCIOPs under the magnetic field in the rats in different groups. The femoral head of the GC group demonstrated significant changes as compared to that of the control group, including the loss of bone minerals in the subchondral area of the femoral head and the occurrence of cystic changes (Figure 6A). Consistent with the data of bone mass formation on micro CT, histological evidence based on HE staining also showed obvious osteonecrosis, sparse and thin bone trabeculae in the femoral head, bone mineral loss in the subchondral area of the femoral head, and abnormal cystic changes in the GC group (Figure 6B).

The bone tissue of the femoral head was analyzed by micro CT, and Figure 6C shows the detection indicators (BMD, BV, BV/TV, Tb. Th, and Tb. Sp). After the treatment of SCIOPs under a magnetic field, the trabeculae in the subchondral area of the femoral head appeared to be complete and evenly distributed with slight changes in osteonecrosis; this effect was better than that of MSCs and SCIOPs alone. The quantitative analysis results of micro CT parameters further proved that SCIOPs under the action of the magnetic field had an optimal therapeutic effect on GC-ONFH. The current study showed that the BMD of the control group was 487±0.029 mg/cm,^{3} that of the GC group was 190±0.018 mg/cm,^{3} and that of SCIOPs under the magnetic field was 392.5±0.025 mg/cm.^{3} Thus, a trend of recovery after treatment was exhibited by the bone tissues in the femoral head, and the density and thickness of bone trabecula were increased, which was more than that of the control group. The above results showed that the particle-loaded

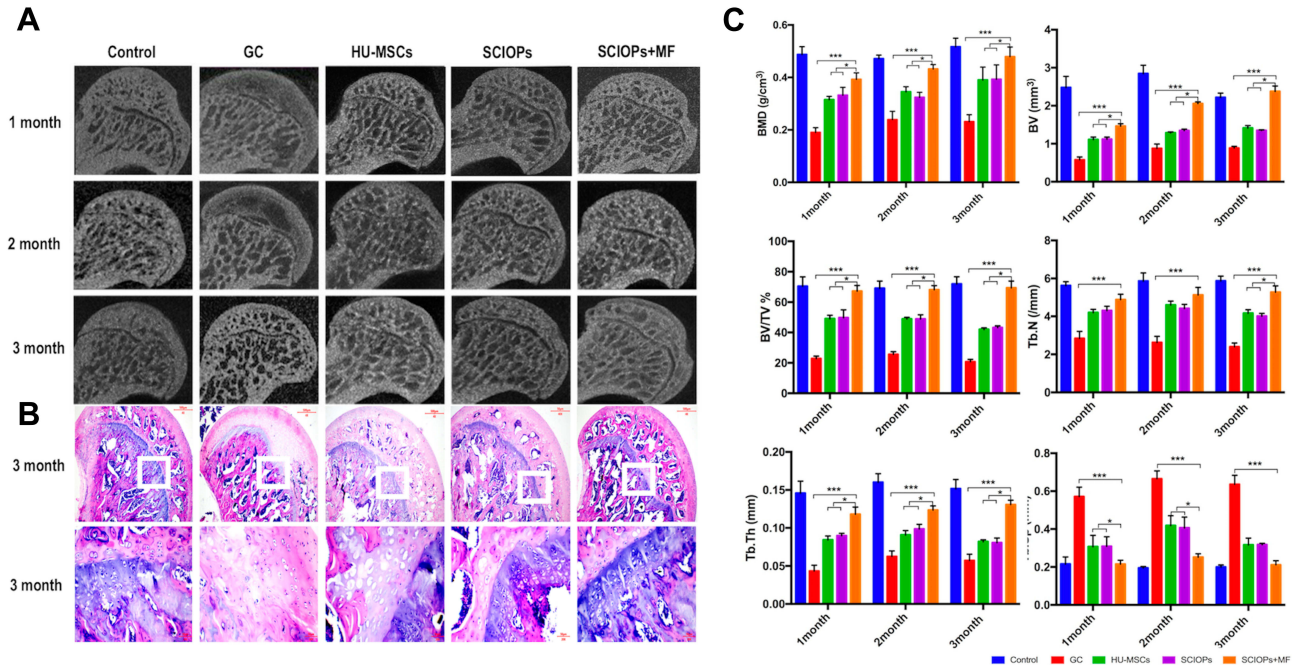

Figure 6 The osteogenesis-promoting effects of SCIOPs+ MF on the rat model of GC-ONFH. (**A**) Reconstructed coronal images of bones within the control, GC, HU-MSCs, SCIOPs, and SCIOPs+ MF groups. (**B**) HE staining of the femoral heads in rats receiving different treatments. Scale bar: 500 μm. (**C**) Quantitative analyses of bone mineral density (BMD), bone volume (BV), bone volume per total volume (BV/TV), trabecular number (Tb. (N), trabecular thickness (Tb. Th), and trabecular separation (Tb. Sp) in the different treatment groups. Bar represents the SD, ***$P < 0.001$, *$P < 0.05$, vs the GC group.

stem cells had effectively restored osteogenesis of the femoral head under the guidance of the magnetic field, showing an increase in the bone formation content. In this non-invasive way and under the intervention of the magnetic field, the stem cells effectively repaired the femoral head and promoted the enhancement of osteogenesis.

We performed the fluorescence microscope (BX51T-PHD-J11; Olympus Corporation, Tokyo, Japan) observation on month's femoral head section and found that the cells marked with CM-Dil in the femoral head. The fluorescence intensity and density of the SCIOPs combined magnetic field targeting group were the highest. The results (Fig S2) showed that under the effect of the magnetic field, the number of SPION@PDA labeled MSCs entering the femoral head increased, and the targeting effect of the magnetic field enhanced the ability of SPION @ PDA labeled MSC to homing into the damaged femoral head.

Cytokines Level

The level of cytokines in the serum of rats at 1, 2, and 3 months after treatment was measured by Luminex, along with the expression level of pro-inflammatory cytokines, TNF-α, IL-1β, and IL-6 and anti-inflammatory cytokines, IL-4 and IL-10. As shown in Figure 7, the anti-inflammatory cytokines, IL-4 and IL-10, in SCIOPs under magnetic field group were significantly higher and the pro-inflammatory cytokines, TNF-α and IL-6, were significantly lower as compared to those in the positive control group. Compared to MSCs and SCIOPs groups, the results showed a higher expression of anti-inflammatory cytokines and lower expression of pro-inflammatory cytokines, albeit the differences were not statistically significant. Therefore, the treatment of GC-ONFH showed increased BMD and trabecular volume of SCIOPs in the magnetic field group, which might be related to the increase in anti-inflammatory cytokines and the decrease in pro-inflammatory cytokines. This also indicated that more stem cells might be homing to the lesion site in SCIOPs under magnetic field group, resulting in decreased pro-inflammatory cytokines and increased anti-inflammatory cytokines. In a pro-inflammatory environment, the cytokine coordination and overlapped signaling pathways enhance the formation of osteoclasts,[31] which leads to the imbalance of osteogenesis and osteoclast, thereby causing osteonecrosis. Therefore, it can be speculated that the increased anti-inflammatory cytokines and decreased pro-inflammatory cytokines assist in the inhibition of aseptic inflammation caused by ONFH to restore the balance of bone repair in the femoral head. In addition to bone cells, macrophages are also involved in the bone microenvironment during the

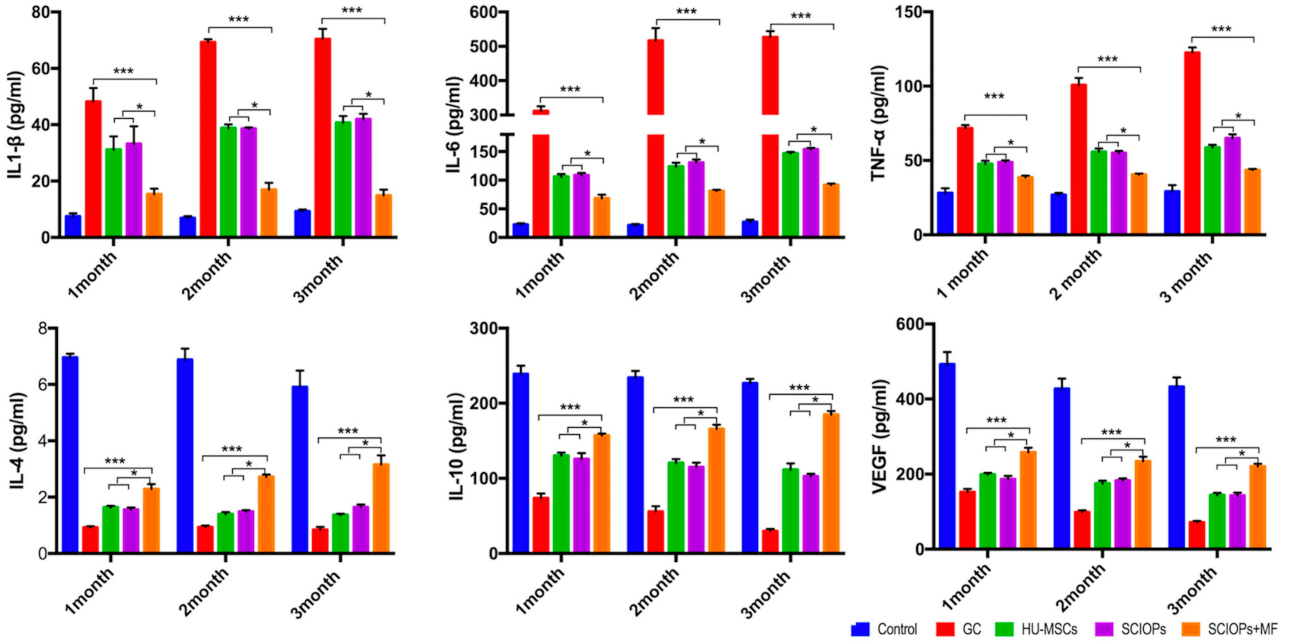

Figure 7 Dynamics of cytokine levels in serum of the GC-ONFH rats (1-, 2-, 3-month) treated with Control, GC, HU-MSCs, SCIOPs, and SCIOPs+ MF. Bar represents the SD, ***$P < 0.001$, *$P < 0.05$, vs the GC group.

development of GC-ONFH.[32] The macrophages could be released from the bone marrow to the circulatory system, and then secrete cytokines. Therefore, under the condition of GC-ONFH, it is also necessary to detect the level of cytokines in serum for evaluating the disease. As macrophages respond to various signals in the damaged tissues and polarize to M1 and M2 macrophages, the dynamic balance during the developmental process of M1 and M2 macrophages determines the development of the disease.[33] M1 macrophages secrete high levels of pro-inflammatory cytokines (such as TNF-α, IL-1β, and IL-6) to promote inflammation,[34,35] while M2 macrophages secrete anti-inflammatory cytokines (IL-10, TGF-β, and IL-4) that facilitate the regression of inflammation. Among these pro-inflammatory cytokines, IL-6 and TNF-α are widespread in the ONFH. TNF-α acts as an effective osteoclast generating factor, which in turn, promotes osteoclast formation and inhibits osteoblast formation. In addition, the elevated level of TNF-α promotes the polarization of a large amount of M1 macrophages, leading to increased expression levels of pro-inflammatory cytokines.[33] However, the high expression of IL-4 was beneficial in reducing the TNF-α level, which inhibits the local inflammatory response and osteonecrosis. Also, IL-4 reduces the activity of caspase-3 in osteonecrosis process.[36] Therefore, the upregulated anti-inflammatory cytokine IL-4 not only inhibits the pro-inflammatory cytokines but also the activity of intracellular apoptotic proteins. IL-10 reduces the activation level of M1 macrophages,[37] thus avoiding excess secretion of pro-inflammatory cytokines. Moreover, VEGF was also detected in this study. It is an angiogenic factor that enhances the angiogenesis of the damaged area through the receptor and multiple signaling pathways, thus contributing to the recovery of osteonecrosis.[38] The results of this study showed that SCIOPs under magnetic field group enhance the potential of stem cells in inhibiting inflammation and repairing tissues, increase the level of VEGF and anti-inflammatory factors, and decrease that of pro-inflammatory factors, which is conducive to the tissue repair of osteonecrosis.

Osteogenic Factors and Apoptotic Protein Changes

In addition to the changes in the inflammatory factors in the serum, the formation of Runx-2 and Osterix was also antagonized in GC-ONFH. The expression levels of Runx-2 and Osterix, critical factors in the promotion of osteogenesis, represents the level of osteogenesis. In SCIOPs under the magnetic field group, the expression of Runx-2 and Osterix was significantly upregulated. Notably, Runx-2 and Osterix were antagonized in GC-ONFH.[17] The current study investigated the 3rd month protein level of Runx-2 and Osterix, and the gene levels at 1, 2, and 3 months. Compared with the positive control group, the expression of osteogenic genes in the SCIOPs combined magnetic field targeting group was

significantly up-regulated, showing obvious differences, indicating that after treatment, bone formation in the femoral head was promoted, which is beneficial to control bone loss in the femoral head. When compared with the MSC group and the SCIOPs group, the SCIOPs combined magnetic field targeting group also showed differences. The results showed that the stem cells repair the ONFH by promoting the osteogenesis of the femoral head under the guidance of the magnetic field (Figure 8A and B). In addition, Runx-2 and Osterix, which are important transcription factors in the process of osteogenesis, also play a role in coordinating the morphological changes and maturation of osteoblasts. The expression of Runx-2 and Osterix plays a key role in osteogenic differentiation and was upregulated in the treatment group, indicating a favorable effect on bone repair and new bone formation.

However, the effective bone repair of GC-ONFH in the treatment group not only depends on the upregulation of osteogenic genes but also on the increased expression of apoptosis-inhibiting proteins, Akt and Bcl-2, and the decreased expression of apoptosis-promoting proteins, Bad and caspase-3. Weinstein et al demonstrated that the apoptosis of osteocytes was only observed during the development of GC-ONFH but not in the posttraumatic ONFH. The study also detected apoptosis of extensive osteoblasts and osteoblasts near the necrotic area,[9] further cementing the inflammatory reactions in the bone tissues if the apoptotic cells existed persistently,[39,40] thus proposing that continuous accumulation would lead to the formation of irreparable defects, leading to joint collapse.[41] Al Dujaili et al reported that apoptosis in osteocytes regulates osteoclast differentiation, which enhances bone absorption.[42] In the treatment group, upregulated Akt and Bcl-2 decreased the activity of caspase by inhibiting Bad. Therefore, avoiding apoptosis of osteoblasts and osteocytes plays a decisive role in the process of bone repair of GC-associated osteonecrosis.

Western blot was conducted to show the 3rd month apoptosis protein level, and the 1-, 2-, and 3-month gene levels were detected by q-PCR assay. The results showed that the treatment of SCIOPs under magnetic field played a key protecting role against GC-ONFH-induced apoptosis through Akt/Bcl-2/Bad/caspase-3 signaling pathway (Figure 9A and B). The phosphorylation and activation of Akt inactivates the apoptosis-promoting protein Bad, and then, the phosphorylation state of inactivated Bad activates Bcl-2 protein.[43] Mitochondrial-dependent Bcl-2 family proteins (Bcl-2 and Bad) and activated caspase-3 play critical roles in the process of apoptosis.[44,45] Bcl-2 is an anti-apoptotic protein, localized on the membrane of mitochondria. The regulation of the mitochondrial outer membrane permeability (MOMP) inhibits the formation of mitochondrial channels that induce apoptosis. This prevents the release of cytochrome c from mitochondria to avoid its transfer from mitochondria to the cytoplasm to activate caspase-3 that induces apoptosis. Caspase-3 belongs to cysteinyl aspartate specific proteinase (caspase) family and can be activated during apoptosis through internal or external pathways. Akt signaling pathway is involved in a variety of cell functions, including cell survival and proliferation. The phosphorylation Akt (p-Akt) upregulates the level of Bcl-2 protein and downregulates the levels of cleaved-caspase-3 protein. Western blotting results revealed that p-Akt was upregulated. The increase levels of p-Akt led to increased apoptosis that inhibits Bcl-2 protein, while decreased apoptosis induces Bad and caspase-3/cleaved-caspase-3 proteins. q-PCR was conducted to further determine the expression level of apoptotic-related genes *Bcl-2/Bad/caspase-3* (Figure 9B). The results showed that the expression level of anti-

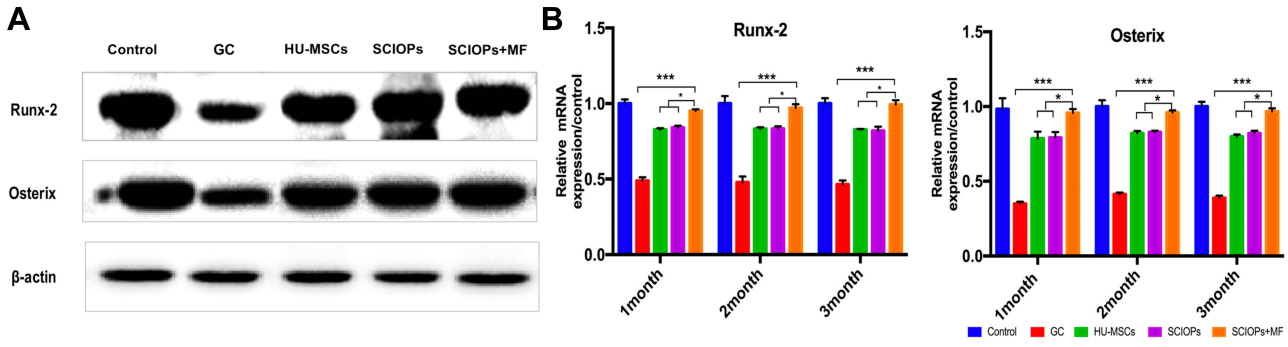

Figure 8 (**A**) Western blot analysis of the expression of Runx-2 and Osterix (third month) in the bone tissue from the five groups. (**B**) RT-PCR shows the mRNA expression level of *Runx-2* and *Osterix* of 1-, 2-, and 3-month bone tissue.(n = 3, bar represents the SD. ***$P < 0.001$, *$P < 0.05$, vs the GC group).

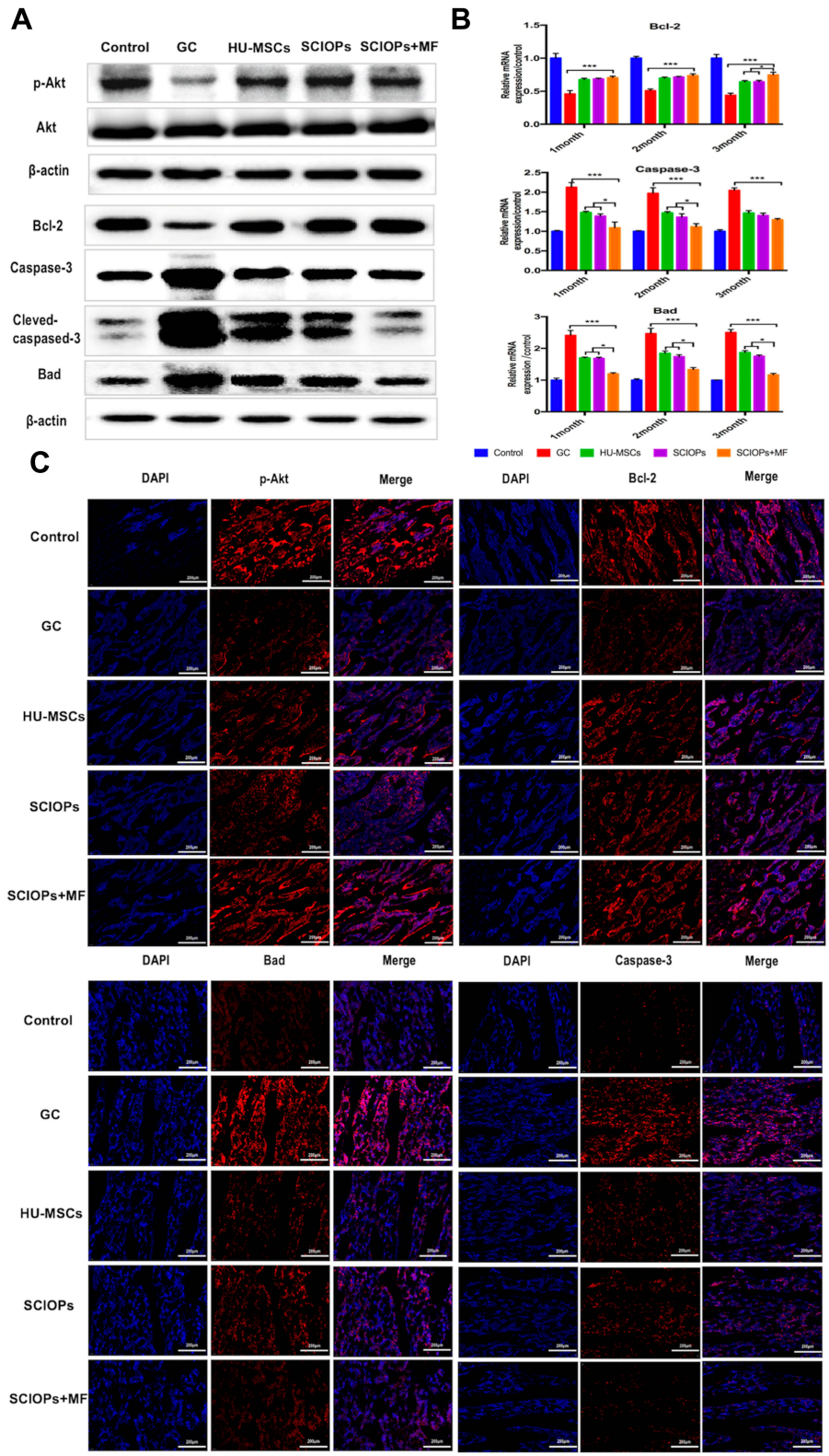

Figure 9 Expression levels of apoptosis proteins. (**A**) In the different treatment groups, the p-Akt Bcl-2, and Bad caspase-3 protein expression levels were examined by Western blotting. (**B**) In the different treatment groups, the *Bcl-2*, *Bad*, and *caspase-3* mRNA expression levels were examined by RT-PCR. Bar represents the SD, ***$P < 0.001$, *$P < 0.05$, vs the GC group. (**C**) The immunofluorescence indicated the expression level of p-Akt, Bcl-2, Bad, and caspase-3 in the bone tissue from the different treatment groups (third month). Scale bar: 200 μm.

apoptotic gene *Bcl-2* was increased and that of the apoptotic gene *Bad/caspase* was decreased in the SCIOPs under magnetic field treatment group compared with the GC group. To investigate the distribution of apoptosis proteins at the necrotic sites, immunofluorescence by double staining of the 3rd month samples was conducted. Figure 9C shows the expression of apoptosis proteins in the bone area. Compared to the GC group, the results indicated that the expression level of Akt/Bcl-2/Bad/caspase-3 in SCIOPs under the magnetic field group was significantly different.

In conclusion, SCIOPs under the magnetic field inhibited apoptosis mainly through Akt/Bcl-2/Bad/caspase-3 pathway and also treated apoptosis and osteogenic dysfunction induced by GC-ONFH by upregulating the expression of osteogenic genes, *Runx-2* and *Osterix*.

Toxicity Test

The potential toxicity of SPION@PDA NPs was evaluated by HE staining analysis of the main organs of rats in all the five groups. No morphological changes were detected in the heart, liver, spleen, lung, and kidney after 3 months of MSC treatment as compared to the control group (Fig S3). This indicated that SPION@PDA NPs have a low toxicity in vivo.

Conclusion

In this study, HU-MSCs-SPION@PDA NPs system was constructed under the action of a magnetic field to treat GC-ONFH. The apoptosis of bone cells was inhibited through the Akt/Bcl-2/Bad/Caspase-3 signaling pathway, the osteogenic function was enhanced, and the bone repair was promoted by the increased expression of osteogenic-related proteins Runx-2 and Osterix. Thus, the current study provided a novel strategy for treating GC-ONFH.

Acknowledgments

This study was supported by the Jilin Province Development and Reform Commission Project (Grant No. 2019C049-8), the Jilin Province Science and Technology Development Plan Project (Grant Nos. 20190901007JC, 20190304030YY and 20190908002TC), the Changchun Science and Technology Development Plan Project (Grant No. 18YJ011), the Bethune project of Jilin University (No.2018A03).

Disclosure

The authors report no conflicts of interest in this work.

References

1. Liu YF, Chen WM, Lin YF, et al. Type II collagen gene variants and inherited osteonecrosis of the femoral head. *N Engl J Med*. 2005; 352 (22):2294–2301. doi:10.1056/NEJMoa042480
2. Cui L, Zhuang Q, Lin J, et al. Multicentric epidemiologic study on six thousand three hundred and ninety five cases of femoral head osteonecrosis in China. *Int Orthop*. 2016; 40(2):267–276. doi:10.1007/s00264-015-3061-7
3. Huang Z, Cheng C, Cao B, et al. Icariin protects against glucocorticoid-induced osteonecrosis of the femoral head in rats. *Cell Physiol Biochem*. 2018; 47(2):694–706. doi:10.1159/000490023
4. Zhang YL, Yin JH, Ding H, Zhang W, Zhang CQ, Gao Y-S. Vitamin K2 prevents glucocorticoid-induced osteonecrosis of the femoral head in rats. *Int J Biol Sci*. 2016; 12(4):347–358. doi:10.7150/ijbs.13269
5. Jiang Y, Zhang Y, Zhang H, et al. Pravastatin prevents steroid-induced osteonecrosis in rats by suppressing PPARgamma expression and activating Wnt signaling pathway. *Exp Biol Med*. 2014; 239:347–355.
6. Chen S, Li J, Peng H, Zhou J, Fang H. Administration of erythropoietin exerts protective effects against glucocorticoid-induced osteonecrosis of the femoral head in rats. *Int J Mol Med*. 2014; 33:840–848.
7. Tao SC, Yuan T, Rui BY, Zhu ZZ, Guo SC, Zhang CQ. Exosomes derived from human platelet-rich plasma prevent apoptosis induced by glucocorticoid-associated endoplasmic reticulum stress in rat osteonecrosis of the femoral head via the Akt/Bad/Bcl-2 signal pathway. *Theranostics*. 2017; 7:733–750.
8. Kerachian MA, Harvey EJ, Cournoyer D, Chow TY, Nahal A, Seguin C. A rat model of early stage osteonecrosis induced by glucocorticoids. *J Orthop Surg Res*. 2011; 6:62.
9. Weinstein RS, Nicholas RW, Manolagas SC. Apoptosis of osteocytes in glucocorticoid-induced osteonecrosis of the hip. *J Clin Endocrinol Metab*. 2000; 85:2907–2912.
10. Youm YS, Lee SY, Lee SH. Apoptosis in the osteonecrosis of the femoral head. *Clin Orthop Surg*. 2010; 2(4):250–255. doi:10.4055/cios.2010.2.4.250
11. Weinstein RS, Jilka RL, Parfitt AM, Manolagas SC. Inhibition of osteoblastogenesis and promotion of apoptosis of osteoblasts and osteocytes by glucocorticoids. potential mechanisms of their deleterious effects on bone. *J Clin Invest*. 1998; 102(2):274–282. doi:10.1172/JCI2799
12. Takano-Murakami R, Tokunaga K, Kondo N, et al. Glucocorticoid inhibits bone regeneration after osteonecrosis of the femoral head in aged female rats. *Tohoku J Exp Med*. 2009; 217(1):51–58. doi:10.1620/tjem.217.51
13. O'Brien CA, Jia D, Plotkin LI, et al. Glucocorticoids act directly on osteoblasts and osteocytes to induce their apoptosis and reduce bone formation and strength. *Endocrinology*. 2004; 145(4):1835–1841. doi:10.1210/en.2003-0990
14. Boya P, Cohen I, Zamzami N, Vieira HL, Kroemer G. Endoplasmic reticulum stress-induced cell death requires mitochondrial membrane permeabilization. *Cell Death Differ*. 2002; 9(4):465–467. doi:10.1038/sj.cdd.4401006
15. Green DR. The pathophysiology of mitochondrial cell death. *Science*. 2004; 305(5684):626–629. doi:10.1126/science.1099320
16. Pattingre S, Tassa A, Qu X, et al. Bcl-2 antiapoptotic proteins inhibit beclin 1-dependent autophagy. *Cell*. 2005; 122(6):927–939. doi:10.1016/j.cell.2005.07.002
17. Ducy P, Zhang R, Geoffroy V, Ridall AL, Karsenty G. Osf2/Cbfa1: a transcriptional activator of osteoblast differentiation. *Cell*. 1997; 89 (5):747–754. doi:10.1016/S0092-8674(00)80257-3
18. Fakhry M. Molecular mechanisms of mesenchymal stem cell differentiation towards osteoblasts. *World J Stem Cells*. 2013; 5 (4):136–148. doi:10.4252/wjsc.v5.i4.136

19. Rackwitz L, Eden L, Reppenhagen S, et al. Stem cell- and growth factor-based regenerative therapies for avascular necrosis of the femoral head. *Stem Cell Res Ther*. 2012; 3(1):7. doi:10.1186/scrt98
20. Hernigou P, Beaujean F. Treatment of osteonecrosis with autologous bone marrow grafting. *Clin Orthop Relat Res*. 2002; 405:14–23. doi:10.1097/00003086-200212000-00003
21. Wang HS, Hung SC, Peng ST, et al. Mesenchymal stem cells in the Wharton's jelly of the human umbilical cord. *Stem Cells*. 2004; 22 (7):1330–1337. doi:10.1634/stemcells.2004-0013
22. Fu YS, Cheng YC, Lin MYA, et al. Conversion of human umbilical cord mesenchymal stem cells in Wharton's jelly to dopaminergic neurons in vitro: potential therapeutic application for parkinsonism. *Stem Cells*. 2006; 24(1):115–124. doi:10.1634/stemcells.2005-0053
23. Huang Z, Shen Y, Sun A, et al. Magnetic targeting enhances retrograde cell retention in a rat model of myocardial infarction. *Stem Cell Res Ther*. 2013; 4(6):149–162. doi:10.1186/scrt360
24. Wu L, Zhang F, Wei Z, et al. Magnetic delivery of Fe3O4@polydopamine nanoparticle-loaded natural killer cells suggest a promising anticancer treatment. *Biomater Sci*. 2018; 6 (10):2714–2725. doi:10.1039/C8BM00588E
25. Li X, Wei Z, Lv H, et al. Iron oxide nanoparticles promote the migration of mesenchymal stem cells to injury sites. *Int J Nanomed*. 2019; 14:573–589. doi:10.2147/IJN.S184920
26. Li X, Wei Z, Li B, et al. In vivomigration of Fe3O4 @polydopamine nanoparticle-labeled mesenchymal stem cells to burn injury sites and their therapeutic effects in a rat model. *Biomater Sci*. 2019; 7 (7):2861–2872. doi:10.1039/C9BM00242A
27. Ge R, Li X, Lin M, et al. Fe3O4 @polydopamine composite theranostic superparticles employing preassembled Fe3O4 nanoparticles as the core. *ACS Appl Mater Interfaces*. 2016; 8(35):22942–22952. doi:10.1021/acsami.6b07997
28. Si J, Yang H. Preparation and characterization of bio-compatible Fe3O4@ Polydopamine spheres with core/shell nanostructure. *Mater Chem Phys*. 2011; 128(3):519–524. doi:10.1016/j.matchemphys.2011.03.039
29. Liu R, Guo Y, Odusote G, Qu F, Priestley RD. Core–Shell Fe3O4 polydopamine nanoparticles serve multipurpose as drug carrier, catalyst support and carbon adsorbent. *ACS Appl Mater Interfaces*. 2013; 5(18):9167–9171. doi:10.1021/am402585y
30. Wightman RM, Amatorh C, Engstrom RC, et al. Real-time characterization of dopamine overflow and uptake in the rat striatum. *Neuroscience*. 1988; 25(2):513–523. doi:10.1016/0306-4522(88)90255-2
31. Feng T, Ji W, Tang Q, et al. Low-fouling nanoporous conductive polymer-coated microelectrode for in vivo monitoring of dopamine in the rat brain. *Anal Chem*. 2019; 91(16):10786–10791. doi:10.1021/acs.analchem.9b02386
32. Zhang Y-H, Heulsmann A, Tondravi MM, Mukherjee A, Abu-Amer Y. Tumor necrosis Factor-α (TNF) stimulates RANKL-induced osteoclastogenesis via coupling of TNF type 1 receptor and RANK signaling pathways. *J Biol Chem*. 2001; 276(1):563–568. doi:10.1074/jbc.M008198200
33. Wang FS, Chung PC, Lin CL, et al. MicroRNA-29a protects against glucocorticoid-induced bone loss and fragility in rats by orchestrating bone acquisition and resorption. *Arthritis Rheum*. 2013; 65 (6):1530–1540. doi:10.1002/art.37948
34. Wu X, Xu W, Feng X, et al. TNF-a mediated inflammatory macrophage polarization contributes to the pathogenesis of steroid-induced osteonecrosis in mice. *Int J Immunopathol Pharmacol*. 2015; 28 (3):351–361. doi:10.1177/0394632015593228
35. Shaul ME, Bennett G, Strissel KJ, Greenberg AS, Obin MS. Dynamic, M2-like remodeling phenotypes of CD11c+ adipose tissue macrophages during high-fat diet-induced obesity in mice. *Diabetes*. 2010; 59(5):1171–1181. doi:10.2337/db09-1402
36. Bouhlel MA, Derudas B, Rigamonti E, et al. PPARγ activation primes human monocytes into alternative M2 macrophages with anti-inflammatory properties. *Cell Metab*. 2007; 6(2):137–143. doi:10.1016/j.cmet.2007.06.010
37. Wu X, Feng X, He Y. IL-4 administration exerts preventive effects via suppression of underlying inflammation and TNF-α-induced apoptosis in steroid-induced osteonecrosis. *Osteoporosis Int*. 2016; 27(5):1827–1837. doi:10.1007/s00198-015-3474-6
38. Villalta SA, Rinaldi C, Deng B, Liu G, Fedor B, Tidball JG. Interleukin-10 reduces the pathology of mdx muscular dystrophy by deactivating M1 macrophages and modulating macrophage phenotype. *Hum Mol Genet*. 2011; 20(4):790–805. doi:10.1093/hmg/ddq523
39. Bao P, Kodra A, Tomic-Canic M, Golinko MS, Ehrlich HP, Brem H. The role of vascular endothelial growth factor in wound healing. *J Surg Res*. 2009; 153(2):347–358. doi:10.1016/j.jss.2008.04.023
40. Weinstein RS. Glucocorticoid-induced bone disease. *N Engl J Med*. 2011; 365(1):62–70. doi:10.1056/NEJMcp1012926
41. Weinstein RS. Glucocorticoid-induced osteoporosis and osteonecrosis. *Endocrinol Metab Clin North Am*. 2012; 41 (3):595–611. doi:10.1016/j.ecl.2012.04.004
42. Mutijima E, De Maertelaer V, Deprez M, Malaise M, Hauzeur J-P. The apoptosis of osteoblasts and osteocytes in femoral head osteonecrosis: its specificity and its distribution. *Clin Rheumatol*. 2014; 33 (12):1791–1795. doi:10.1007/s10067-014-2607-1
43. Al-Dujaili SA, Lau E, Al-Dujaili H, Tsang K, Guenther A, You L. Apoptotic osteocytes regulate osteoclast precursor recruitment and differentiation in vitro. *J Cellul Biochem*. 2011; 112(9):2412–2423. doi:10.1002/jcb.23164
44. Yu F, Sugawara T, Maier CM, Hsieh LB, Chan PH. Akt/Bad signaling and motor neuron survival after spinal cord injury. *Neurobiol Dis*. 2005; 20(2):491–499. doi:10.1016/j.nbd.2005.04.004
45. Alnemri ES, Livingston DJ, Nicholson DW, et al. Human ICE/CED-3 protease nomenclature. *Cell*. 1996; 87(2):171. doi:10.1016/S0092-8674(00)81334-3
46. Woo SH, Park IC, Park MJ, et al. Arsenic trioxide induces apoptosis through a reactive oxygen species-dependent pathway and loss of mitochondrial membrane potential in HeLa cells. *Int J Oncol*. 2002; 21:57–63.

International Journal of Nanomedicine Dovepress

Publish your work in this journal

The International Journal of Nanomedicine is an international, peer-reviewed journal focusing on the application of nanotechnology in diagnostics, therapeutics, and drug delivery systems throughout the biomedical field. This journal is indexed on PubMed Central, MedLine, CAS, SciSearch®, Current Contents®/Clinical Medicine, Journal Citation Reports/Science Edition, EMBase, Scopus and the Elsevier Bibliographic databases. The manuscript management system is completely online and includes a very quick and fair peer-review system, which is all easy to use. Visit http://www.dovepress.com/testimonials.php to read real quotes from published authors.

Submit your manuscript here: https://www.dovepress.com/international-journal-of-nanomedicine-journal